Detectability Models for Multiple Access Low-Probability-of-Intercept Networks

ROBERT F. MILLS
Air Force Institute of Technology

GLENN E. PRESCOTT, Senior Member, IEEE
University of Kansas

Increased demands for communications in the tactical battlefield have driven the development of multiple access low-probability-of-intercept (LPI) networks. Most detectability studies of LPI networks focus on the individual links of the network, in which the intercept and detectability calculations are conducted for a single network transmitter. We assume here that the interceptor does not attempt to distinguish one emitter from another, but rather focuses on the operational status of the network so that LPI network performance quality metrics can be established.

Manuscript received July 3, 1998; revised November 9, 1999; released for publication April 10, 2000.

IEEE Log No. T-AES/36/3/07803.

Refereeing of this contribution was handled by T. F. Roome.

Authors' addresses: R. F. Mills, formerly with the Department of Electrical and Computer Engineering, Air Force Institute of Technology, Wright-Patterson AFB, OH 45433; G. E. Prescott, Department of Electrical Engineering and Computer Science, University of Kansas, Lawrence, KS 66045, e-mail: (prescott@ukans.edu).

I. INTRODUCTION

The concept of multiple access low-probability-of-intercept (LPI) networks has generated considerable interest in the past few years, due to increased demands for highly connected, yet covert, communications in the tactical battlefield. A number of research efforts have concentrated on network design issues, such as throughput, packet switching, and message routing, while others have focused on the detectability of the network links. However, these detectability analyses have traditionally emphasized the interception of a single network transmitter, as opposed to the network at large.

This work presents a different approach to detectability analysis of the LPI network. It is assumed that the interceptor does not attempt to isolate a particular emitter, but instead decides whether or not a network is currently operational. Hence, detection of the network may be based on energy received from either a single or multiple transmitters.

The candidate network considered here uses frequency hop code division multiple access (FH-CDMA), in which users are assigned orthogonal frequency hop patterns. The total network bandwidth is defined as W_1, and the network "on-time" is T_1 seconds. The network has $M = W_1/W_2$ contiguous channels, and uses a hop rate of $1/T_2 = N/T_1$ hops/s. Omnidirectional communications antennas are assumed. The two intercept receivers used here are the wideband radiometer, which forms a detection decision based on a single energy measurement on the $T_1 \times W_1$ time-frequency space, and the channelized radiometer (Fig. 1), which makes NM energy measurements on smaller time-frequency cells $T_2 \times W_2$, which are then combined to form an overall decision.

II. DISPERSED NETWORK INTERCEPT MODEL

A. Intercept Links

Fig. 2 shows a generic network intercept scenario, which is described here as the dispersed network intercept model. It differs from simple link intercept scenarios in that the interceptor has the ability to collect and process energy from multiple sources in the communications network. The total received input to the intercept receiver is

$$x(t) = \sum_{j=1}^{U} s_j(t) + \sum_{k=1}^{N} J_k(t) + n(t) \tag{1}$$

where $s_j(t)$ is the received signal from the jth transmitter, U is the number of active transmitters, and $n(t)$ is additive white Gaussian noise (AWGN) with two-sided power spectral density $N_0/2$. The terms $J_k(t)$ represent N jamming signals.

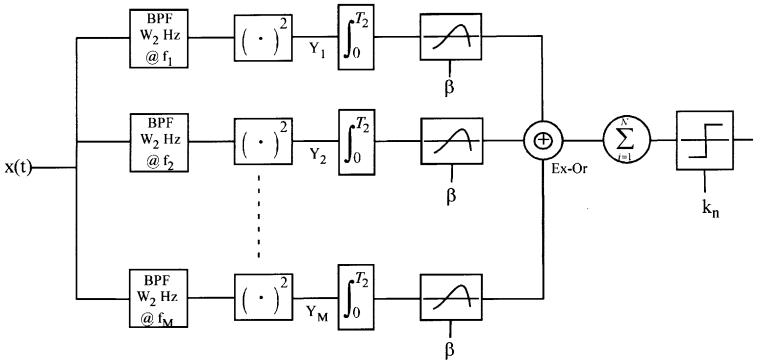

Fig. 1. Channelized radiometer for FH-CDMA networks.

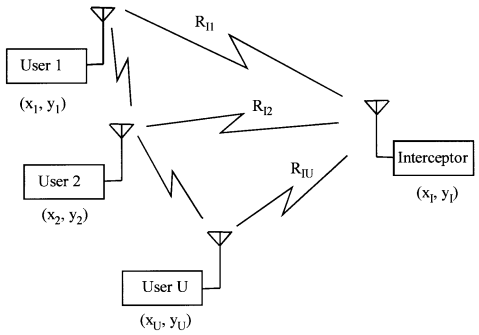

Fig. 2. Distributed network intercept model.

Because the two intercept receivers considered are energy detectors, the received energy from each network transmitter must be determined. The average power received at the interceptor at a distance R_{Ij} from the jth transmitter is given as follows:

$$S_{Ij} = \frac{P_{Tj} G_{TjI} G_{ITj}}{\alpha_{Ij}(f, R_{Ij}) L_{Ij}} \tag{2}$$

where P_{Tj} is the average power in the signal $s_j(t)$ originating at the jth transmitter, and G_{TjI} and G_{ITj} are the gains of the transmit and intercept antennas, respectively, in the direction of the intercept path. The term $\alpha_{Ij}(f, R_{Ij})$ represents the propagation loss in the jth intercept link, and L_{Ij} accounts for any other path losses, such as atmospheric losses. The energy received from the jth transmitter is then obtained by multiplying by $T_j = \min\{T_I, T_{Sj}\}$, where T_I is the integration time of the interceptor, and T_{Sj} is the duration of the signal. Hence,

$$E_j = \frac{P_{Tj} G_{TjI} G_{ITj} T_j}{\alpha_{Ij}(f, R_{Ij}) L_{Ij}}. \tag{3}$$

The performance of an intercept receiver is often described in terms of its probability of false alarm P_F, probability of detection P_D, and signal-to-noise ratio (SNR). For example, given an acceptable P_F and a desired P_D, the required SNR is usually determined through the use of detection curves or analytic approximations. Likewise, the achievable P_D can be determined given an available SNR and some specified P_F. In any case, the SNR is often expressed as the ratio of energy to noise/interference power spectral density (PSD), as follows:

$$\frac{E_j}{N_{SI}} = \frac{P_{Tj} G_{TjI} G_{ITj} T_j}{\alpha_{Ij}(f, R_{Ij}) L_{Ij} N_{SI}}. \tag{4}$$

The noise plus interference PSD at the intercept receiver N_{SI} accounts for AWGN, with PSD N_{0I}, and any interference (which may be intentional or unintentional). As discussed in [5], $N_{SI} = N_{0I} + N_{JI}$, where

$$N_{0I} = k_B T_{aI} + k_B T_0 (F_I - 1) \tag{5}$$

$$N_{JI} = \sum_{n=1}^{N} \sum_{m=1}^{M} g_{In} g_{Im} \frac{J_{mnI}}{B_I} \tag{6}$$

and k_B is Boltzmann's constant, B_I is the bandwidth of the intercept receiver, T_{aI} is the intercept antenna noise temperature, T_0 is room temperature (290° K), and F_I is the intercept receiver noise figure. Here the jamming PSD accounts for the effects of N jammers, which are assumed to transmit in discrete frequency cells. J_{nmI} represents the power level transmitted by the nth jammer (out of N total) in the mth frequency slot (M total). The factors g_{In} and g_{Im} represent the null-steering and interference suppression factors, respectively, which act together to reduce the effect of J_{nmI}. In a dense jamming environment, N_{SI} will be dominated by the jamming (i.e., $N_{SI} \approx N_{JI}$), while in an interference-free environment, the thermal noise will dominate ($N_{SI} \approx N_{0I}$).

B. Communication Links

Now we examine the communication links in the LPI network. It is assumed that each transmitter may broadcast to several network receivers simultaneously. For the ith receiver located at a distance R_{Cji} from the jth transmitter, the received signal power is

$$S_{Ci} = \frac{P_{Tj} G_{TjCi} G_{CiTj}}{L_{Cji} \alpha_{Cji}(f, R_{Cji})} \tag{7}$$

where P_{Tj} is the average transmit power, G_{TjCi} and G_{CiTj} are the transmit and receive antenna gains in the link, $\alpha_{Cji}(f,R_{Cji})$ is the propagation loss, and L_{Cji} accounts for the atmospheric loss.

As before, we can account for the effects of noise and interference using a combined PSD as shown below,

$$N_{SCi} = N_{0Ci} + N_{JCi} \tag{8}$$

where

$$N_{0Ci} = k_B T_{aCi} + kT_0(F_{Ci} - 1) \tag{9}$$

$$N_{JCi} = \sum_{n=1}^{N}\sum_{m=1}^{M} g_{Cin} g_{Cim} \frac{J_{mnCi}}{B_{Ci}} \tag{10}$$

where g_{Cin} and g_{Cim} represent the null-steering and interference suppression factors for the communication receiver. In a dense environment, $N_{SCi} \approx N_{JCi}$, while in a jam-free environment, $N_{SCi} \approx N_{0Ci}$. Note that each network receiver will likely experience a different amount of interference, based on the antennas, receiver structures, and different jamming levels.

Equation (7) describes the average received signal at a given network receiver. Generally, we are interested in the SNR, usually expressed as a ratio of bit energy to noise/interference PSD, required to obtain some specified bit error probability P_E. Using N_{SC} in (7) and solving for P_{Tj} yields

$$P_{Tj} = \left(\frac{S_{Ci}}{N_{SCi}}\right) \frac{N_{SCi} L_{Cji} \alpha_{Cji}(f,R_{Cji})}{G_{TjCi} G_{CiTj}}. \tag{11}$$

Unfortunately, this equation describes the transmitter power required to deliver a specified SNR (to obtain some specified P_E) at a specific receiver, and each intended receiver would yield a different solution to (11). To overcome this problem, we make some assumptions regarding the LPI network. First, we assume that omnidirectional antennas are used for mobility and broadcast purposes. Hence, all antenna gains are constant:

$$G_{CiTj} = G_{TjCi} = G_{TjI} = G_C. \tag{12}$$

Second, we assume the LPI network receivers operate in essentially the same noise and jamming environment, so $N_{SCi} \approx N_{SC}$. Third, the atmospheric losses L_{Cji} are assumed to be roughly equivalent, since all of the receivers are operating in the same environment. And fourth, we assume that the required SNR at each communication receiver is constant, depending on the desired P_E and the data rate: $S_C/N_{SC} = R_b E_b/N_{SC} = f(P_E)$. Under these assumptions, the required transmitter power depends on the distance to the furthest receiver, and (11) can be rewritten as

$$P_{Tj} = \left(R_b \frac{E_b}{N_{SC}}\right) \frac{N_{SC} L_{Cj} \alpha_{Cj}(f,R_{Cj})}{G_C^2} \tag{13}$$

where $R_{Cj} = \max\{R_{Cji}\}$ is the broadcast range of the transmitter. The transmit power given in (13) ensures that any receiver located within a radius R_{Cj} of the transmitter will have sufficient SNR to achieve or exceed the desired performance requirements. Using (13) in (4) yields

$$\frac{E_j}{N_{SI}} = T_{Sj}\left(R_b \frac{E_b}{N_{SC}}\right) \frac{G_{ITj}}{G_C} \frac{N_{SC}}{N_{SI}} \frac{L_{Cj}}{L_{Ij}} \frac{\alpha_{Cj}(f,R_{Cj})}{\alpha_{Ij}(f,R_{Ij})}. \tag{14}$$

Finally, if the communication and intercept receivers adequately remove any interference and have equivalent noise figures, $N_{SC} \approx N_{SI} = N_0$, and if the atmospheric losses are approximately equal, $L_{Cj} \approx L_{Ij}$. Furthermore, we use the commonly accepted free space propagation loss $\alpha(f,R) = (4\pi fR/c)^2$. Using these assumptions,

$$\frac{E_j}{N_0} = T_{Sj}\left(R_b \frac{E_b}{N_0}\right) \frac{G_{ITj}}{G_C} \left(\frac{R_{Cj}}{R_{Ij}}\right)^2. \tag{15}$$

From this equation, we see several parameters which can be adjusted to minimize the available SNR at the interceptor (and thereby degrade its detection performance). For example, the use of efficient waveforms requiring less E_b/N_0, and shorter communication ranges will render a particular transmitter less detectable. The interception of an LPI network, however, is more complicated, since the interceptor has the ability to process multiple signals.

C. Wideband Radiometer

The wideband radiometer is a noncoherent energy measurement device, whose performance is described by its probability of false alarm P_F, probability of detection P_D, received SNR E/N_0, and time-bandwidth product T_1W_1. For fixed P_F and T_1W_1, there is a one-to-one relationship between the SNR and the probability of detection. For large time-bandwidth products ($T_1W_1 \geq 1000$), the following approximation is sufficient [1]:

$$P_D = Q\left[Q^{-1}(P_F) - \frac{(E/N_0)_{\text{recv}}}{\sqrt{T_1W_1}}\right], \qquad T_1W_1 \geq 1000 \tag{16}$$

where $Q(x)$ is the tail integral of the zero-mean, unit-variance Gaussian density function:

$$Q(x) = \frac{1}{\sqrt{2\pi}} \int_x^\infty e^{-z^2/2}\, dz. \tag{17}$$

Conversely, to obtain a desired P_D, the required SNR is

$$\left(\frac{E}{N_0}\right)_{\text{req}} = [Q^{-1}(P_F) - Q^{-1}(P_D)]\sqrt{T_1W_1}, \qquad T_1W_1 \geq 1000. \tag{18}$$

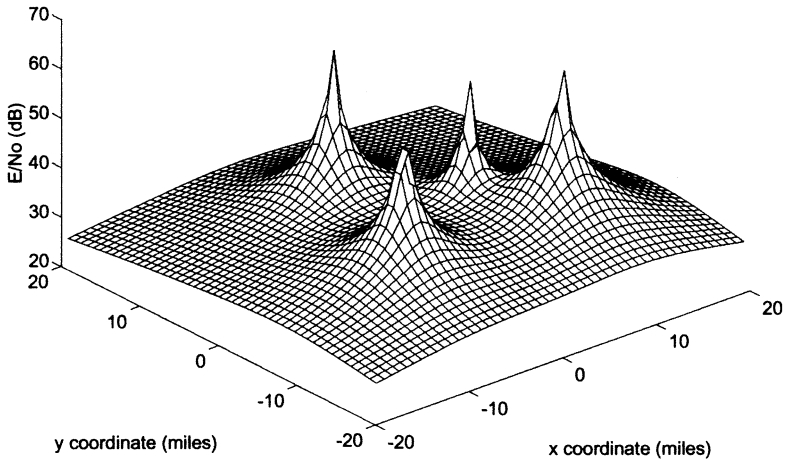

Fig. 3. Received E/N_0 mesh surface.

If the bandwidth of the radiometer covers all signals present in the LPI network, the received energy from all active transmitters determines the achievable probability of detection. The network signals are assumed to be orthogonal by virtue of the assignment of the frequency hop codes, so the total received energy is simply the sum of the energy levels received from each transmitter. For U transmitters located at $\{(x_j, y_j)\}$, the total received SNR at an intercept location (x_I, y_I) is therefore

$$\left(\frac{E}{N_0}\right)_{\text{recv}} = \sum_{j=1}^{U} T_{Sj} \left(R_b \frac{E_b}{N_0}\right) \frac{G_{ITj}}{G_C} \left(\frac{R_{Cj}}{R_{Ij}}\right)^2 \tag{19}$$

$$= \sum_{j=1}^{U} T_{Sj} \left(R_b \frac{E_b}{N_0}\right) \frac{G_{ITj}}{G_C} \frac{R_{Cj}^2}{(x_I - x_j)^2 + (y_I - y_j)^2}. \tag{20}$$

A useful interpretation of (20) is given in Fig. 3, in which the received E/N_0 from four transmitters is represented by a three-dimensional surface above the physical $x-y$ plane. Taking horizontal cuts of the surface yields contours of constant SNR (constant P_D for fixed P_F) as shown in Fig. 4.

Given a desired intercept performance level, the network is detectable if

$$\left(\frac{E}{N_0}\right)_{\text{recv}} \geq \left(\frac{E}{N_0}\right)_{\text{req}} \tag{21}$$

$$\sum_{j=1}^{U} \tau_j \left(\frac{R_{Cj}}{R_{Ij}}\right)^2 \frac{G_{ITj}}{G_C} \geq \frac{S_I/N_0}{S_C/N_0} \tag{22}$$

where $\tau_j = T_{Sj}/T_1$, $S_I/N_0 = (1/T_1)(E/N_0)_{\text{req}}$, and $S_C/N_0 = R_b(E_b/N_0)$. The ratio $(S_I/N_0)/(S_C/N_0)$ is known as the modulation quality factor [3, 5], and quantifies the detectability of a waveform in terms of the specified intercept and communication performance requirements.

Analysis of (22) and Fig. 4 shows that detection of the network can be achieved in two ways. First,

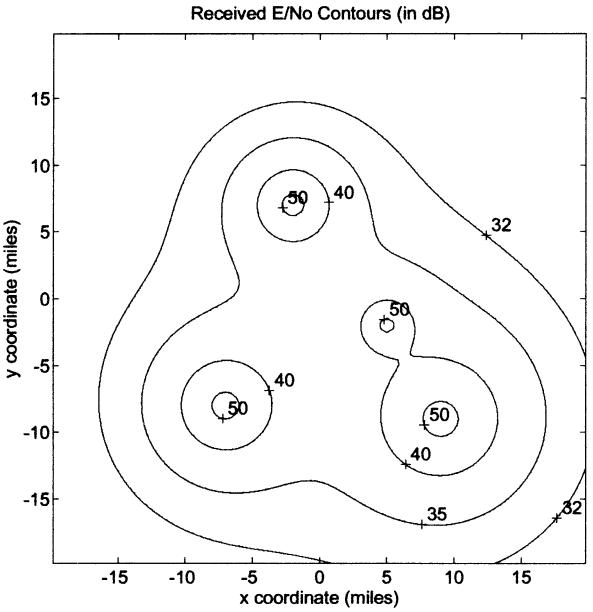

Fig. 4. Received E/N_0 contours.

any single transmitter is detectable if the interceptor is close enough to that transmitter (R_{Ij} is small), as shown by the circular contours around the transmitters. Second, there may also be intermediate regions in which interception is possible due to the reception of energy from multiple sources. In these regions, no single transmitter is detectable by itself, but multiple ones are.

D. Channelized Radiometer

Because signal energy is confined to discrete channels and time slots, the FH-CDMA network is susceptible to detection by pulse detection schemes, such as the channelized radiometer, or filter bank/binary moving window (BMW) detector [1]. The overall network time-frequency space is divided into NM cells with time-bandwidth product T_2W_2,

corresponding to the bandwidth and hop periods of the network signals. Although simply ORing the channel outputs is inefficient in cases where many channels contain signal energy, it is used here to allow detection of as few as one or two transmitters, i.e., it is assumed that the interceptor does not know exactly how many signals might be present.

We assume that the signal and noise statistics are constant for each hop interval T_2, and that the hop decisions are statistically independent. That is, the total energy of a given signal is equally distributed among the N hops, and the number of channels containing signal U is the same from hop to hop. The overall probabilities of false alarm and detection are then given as

$$P_F = \sum_{i=k_N}^{N} \binom{N}{i} p_0^i (1-p_0)^{N-i} \tag{23}$$

$$P_D = \sum_{i=k_N}^{N} \binom{N}{i} p_1^i (1-p_1)^{N-i} \tag{24}$$

where p_0 is the probability that a "1" enters the BMW detector when only noise is present in a T_2 interval, and p_1 is the probability that a "1" enters the window with energy present during that interval. A digital threshold of $k_N = 0.5 - 0.6N$ is usually adequate for BMW detectors [2, 4].

The frequency channels are disjoint, so their noise processes are assumed to be statistically independent, and the false alarm probability, denoted as Q_F, is the same for all channels. Therefore, the probability that one or more channels results in a detection, when in fact no signals are present, is the complement of the probability that none have a false alarm,

$$p_0 = 1 - (1 - Q_F)^M \tag{25}$$

hence, the allowable single channel false alarm probability given a desired P_F is

$$Q_F = 1 - (1 - p_0)^{1/M} \tag{26}$$

where p_0 is solved using (23).

If a channel contains signal, its achievable probability of detection Q_{Dj} depends on the received energy from the network transmitter operating on that channel,

$$Q_{Dj} = Q\left[Q^{-1}(Q_F) - \frac{E_j/N_0}{\sqrt{T_2 W_2}}\right] \tag{27}$$

where E_j/N_0 is given in (15). The probability p_1 then is the probability that one or more channels has a detection, given that U channels actually have signal. This is determined using the complement of the probability that there are no false alarms in the $M-U$ channels containing only noise, and no detections in the U channels containing signal energy:

$$p_1 = 1 - (1 - Q_F)^{M-U} \prod_{j=1}^{U} (1 - Q_{Dj}) \tag{28}$$

which is then used in (24) to determine the overall achieved probability of detection.

E. Performance Metric. Intercept Area

To compare the performance of one intercept receiver with another, or to assess the effect of changes in waveform parameters on network detectability, a performance metric is required. An effective measure of any LPI system, be it a single link or a network of many users, is the expected region of communications compared with the potential region of interception. For simple point-to-point LPI links, intercept range is an appropriate measure, but it is somewhat meaningless in the context of the dispersed network, since each transmitter has its own intercept range.

As can be seen from Fig. 4, intercept area, on the other hand, is an appropriate measure of network detectability for the dispersed LPI network. For a given P_D, or $(E/N_0)_{\text{req}}$ for the radiometer, the intercept area is obtained by integrating the regions enclosed by the appropriate contour lines. Unfortunately, it is difficult, or even impossible, to integrate these regions analytically, except in the most simple cases, such as a single transmitter with circular contours.

The intercept area can be estimated numerically, however, by dividing the geographic region of the network into an $N_X \times N_X$ grid and determining the achievable detection probability for each sample point. An estimate of the intercept area is then determined by counting the number of sample points which exceed the desired P_D, as follows:

$$A_{\text{int}} = \sum_{k=1}^{N_X} \sum_{l=1}^{N_X} \delta_{kl} A_{\text{step}} \tag{29}$$

$$\delta_{kl} = \begin{cases} 1, & P_D(k,l) \geq P_D \\ 0, & P_D(k,l) < P_D \end{cases} \tag{30}$$

where A_{step} is the area of each sample (i.e., step size), and $P_D(k,l)$ is the probability of detection evaluated at the center of the (k,l)th sample point (x_k, y_l). Clearly, smaller step sizes will lead to more accurate results, at the expense of increased computation time.

III. STAND-OFF NETWORK INTERCEPT MODEL

A second network intercept model can be developed for the scenario in which the interceptor is standing-off from a group of emitters which are tightly clustered, or perhaps collocated. This is the stand-off network intercept model. The key

assumptions for the stand-off model are that the ranges from the interceptor to each transmitter are approximately constant ($R_{Ij} = R_I$), and that the intercept gain is approximately constant ($G_{ITj} = G_I$). It is also assumed that the transmitters use equal power ($R_{Cj} = R_C$), and that all signals have the same duration ($T_{Sj} = T_S$). Using these assumptions with (15), we see that the energy received at the interceptor from each transmitter is constant:

$$\frac{E_j}{N_0} = T_S \left(R_b \frac{E_b}{N_0} \right) \frac{G_I}{G_C} \left(\frac{R_C}{R_I} \right)^2. \tag{31}$$

A. Stand-off Radiometer

The radiometer processes the total energy received from all transmitters. Using (31) in (20) yields

$$\left(\frac{E}{N_0} \right)_{\text{recv}} = U T_S \frac{G_I}{G_C} \frac{S_C}{N_0} \left(\frac{R_C}{R_I} \right)^2. \tag{32}$$

The stand-off network intercept scenario is quite similar to the interception of simple point-to-point link, in fact, the collocated network could be interpreted as a single transmitter operating with a higher data rate or power level. Hence, a useful performance metric for the stand-off intercept model is the ratio of the communication range to the intercept range,

$$Q_{RAD} = \left(\frac{R_C}{R_I} \right)^2 = \frac{(S_I/N_0)}{(S_C/N_0)} \frac{G_C}{\tau U G_I} \tag{33}$$

where $\tau = T_S/T_1$, and $(R_C/R_I)^2$ is defined as the network LPI quality factor. The network LPI quality factor is similar in concept to LPI link quality factors discussed in [3, 5]. S_I/N_0 is the SNR required by the interceptor to obtain its desired P_D and P_F, as shown below:

$$\frac{S_I}{N_0} = \frac{1}{T_1} \left(\frac{E}{N_0} \right)_{\text{req}} = [Q^{-1}(P_F) - Q^{-1}(P_D)] \sqrt{\frac{W_1}{T_1}}, \tag{34}$$

$$T_1 W_1 \geq 1000.$$

From (33), we see that adding more users to the network (i.e., increasing U) results in an increase in the detection range R_I. This increase in detectability can be offset by improving the LPI properties of the network waveforms, i.e., by increasing the modulation quality factor $(S_I/N_0)/(S_C/N_0)$.

B. Stand-off Channelized Radiometer

Since equal energy is received from each transmitter, all channels containing signal have the same detection probability. Hence, (28) can be rewritten as follows:

$$Q_{Dj} = Q_D = 1 - \left[\frac{1 - p_1}{(1 - Q_F)^{M-U}} \right]^{1/U} \tag{35}$$

where $Q_F = 1 - (1 - p_0)^{1/M}$, and p_0 and p_1 are obtained from (23) and (24). The required SNR to obtain Q_D and Q_F is

$$\frac{S_I}{N_0} = \frac{1}{T_2} \left(\frac{E}{N_0} \right)_{\text{req}} = [Q^{-1}(Q_F) - Q^{-1}(Q_D)] \sqrt{\frac{W_2}{T_2}}, \tag{36}$$

$$T_2 W_2 \geq 1000.$$

The network LPI quality factor for the channelized detector is then defined as

$$Q_{FB} = \left(\frac{R_C}{R_I} \right)^2 = \frac{(S_I/N_0)}{(S_C/N_0)} \frac{G_C}{\tau G_I} \tag{37}$$

where $\tau = T_S/T_2$.

Comparing (33) and (37), we see that there is not a direct relationship between the number of emitters U and the overall detectability for the channelized radiometer like there is for the wideband radiometer. Instead, the effect of U is more subtle, manifesting itself in (35). Intuitively, however, it is clear that increasing the number of users makes the network more detectable, since more channels are likely to give a detection.

IV. NETWORK WAVEFORM DESIGN

A. Receiver Comparisons

With these detectability models and performance metrics, we can now evaluate the detectability of an LPI network with various waveform parameters. For the dispersed network, our performance metric is simply the area of interception for some specified P_D and P_F. For example, if the area of interception using the channelized radiometer is larger than that for the wideband radiometer, we would conclude that the channelized radiometer poses the greater threat to the LPI network.

In LPI link design, waveform parameters are often selected to prevent the interceptor from gaining any advantage by selecting one type of intercept receiver over another. In fact, the waveform is usually designed such that the wideband radiometer poses the greatest threat to the LPI system. For frequency hopping signals, it has been shown [1, 4] that higher hop rates will defeat the channelized radiometer, and we would therefore expect the same to hold true for interception of the LPI network.

The detectability model for the dispersed network is highly scenario dependent and does not lend itself to a closed-form analysis in which the intercept areas can be easily evaluated as a function of the waveform parameters. However, some insight into network waveform design can be obtained using the stand-off intercept model, in which parameters such as transmitter placement and power levels are no longer scenario-specific. Hence, the performance of the two

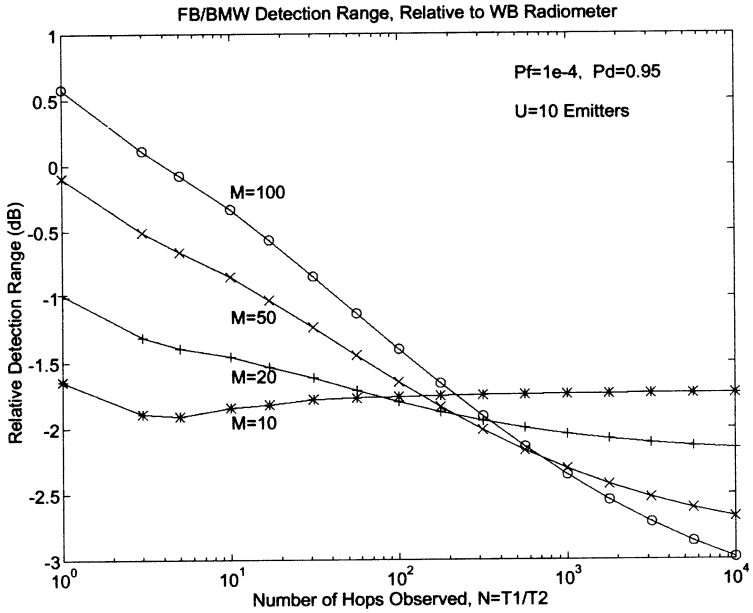

Fig. 5. Effect of hop rate on detection ranges, $U = 10$ emitters.

detectors can be compared using the LPI network quality factors:

$$\frac{Q_{RAD}}{Q_{FB}} = \left(\frac{R_{FB}}{R_{RAD}}\right)^2 = \frac{(S_I/N_0)_{RAD}/U}{(S_I/N_0)_{FB}}$$

$$= \frac{d_{RAD}/U\sqrt{W_1/T_1}}{d_{FB}\sqrt{W_2/T_2}}, \qquad \begin{matrix} T_1W_1 \geq 1000 \\ T_2W_2 \geq 1000 \end{matrix} \tag{38}$$

where R_{RAD} and R_{FB} are the intercept ranges for the wideband and channelized radiometers, respectively, and

$$d_{RAD} = Q^{-1}(P_F) - Q^{-1}(P_D)$$
$$d_{FB} = Q^{-1}(Q_F) - Q^{-1}(Q_D).$$

Substituting $T_2 = T_1/N$ and $W_2 = W_1/M$ into (38) yields

$$\left(\frac{R_{FB}}{R_{RAD}}\right)^2 = \frac{d_{RAD}}{d_{FB}}\frac{1}{U}\sqrt{\frac{M}{N}}. \tag{39}$$

Thus, we see that the relative performance of the two detectors depends on N, M, and U. For constant T_1 and W_1, N and M define the hop rate (i.e., $1/T_2 = N/T_1$ hops/s), and channel bandwidth, W_2, respectively. The bandwidth of the wideband radiometer completely contains all of the network signals, so its performance is independent of N and M.

As shown in Fig. 5, the performance of the channelized detector suffers as the hop rate increases. This is consistent with previous research on the interception of single LPI links, and can be attributed to the reduction in integration time as the hop rate increases. It can be shown that the effect of the hop rate diminishes as the network becomes more heavily loaded. For example, with $U = 10$ and $M = 100$, a factor of 10 change in hop rate results in a decrease in relative detection range of 0.8–0.9 dB. For the fully loaded network, changing the hop rate has little or no effect.

Increasing M decreases the channel bandwidth, favoring the channelized radiometer, as illustrated in Fig. 6. As shown, the channelized radiometer becomes less sensitive to changes in M as the hop rate increases. Note however, that the channelized detector is better than the radiometer ($R_{FB}/R_{RAD} > 0$ dB) only when N and U are small, and M is large.

Adding more users increases the network's detectability with both detectors. However, the radiometer is more sensitive to increases in U. When the network load, U/M, is small, the channelized detector provides better detection performance than the radiometer. However, as the network load increases, the radiometer performs better. As M and N both increase, the load at which the two detectors provide equivalent performance decreases, as shown in Fig. 7.

There are two primary reasons why the filter bank detector is superior only for detection of lightly loaded networks. First, the channelized radiometer is a suboptimal receiver designed for detecting a single frequency hopped signal. Since FH signals occupy only a single channel in any hop interval, the binary ORing of the channel outputs is sufficient. However, if signal energy is present in multiple channels (and if the interceptor knows exactly how many channels) then summation and thresholding of the filter bank outputs, prior to BMW detection over the hop periods, provides better performance. In any case, the radiometer will always be more sensitive when every channel is full, because of binary quantization losses.

From the results in the preceding sections, the wideband radiometer generally presents the greater

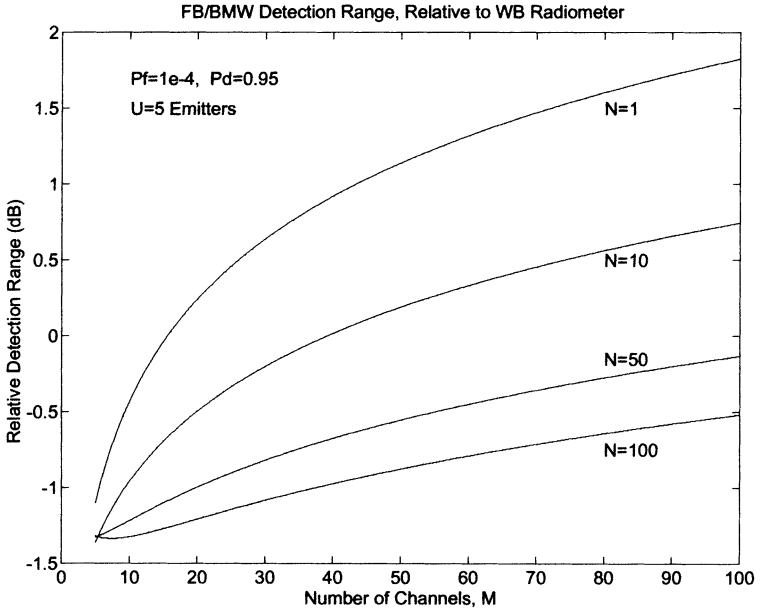

Fig. 6. Effect of number of channels on detection ranges, $U = 5$.

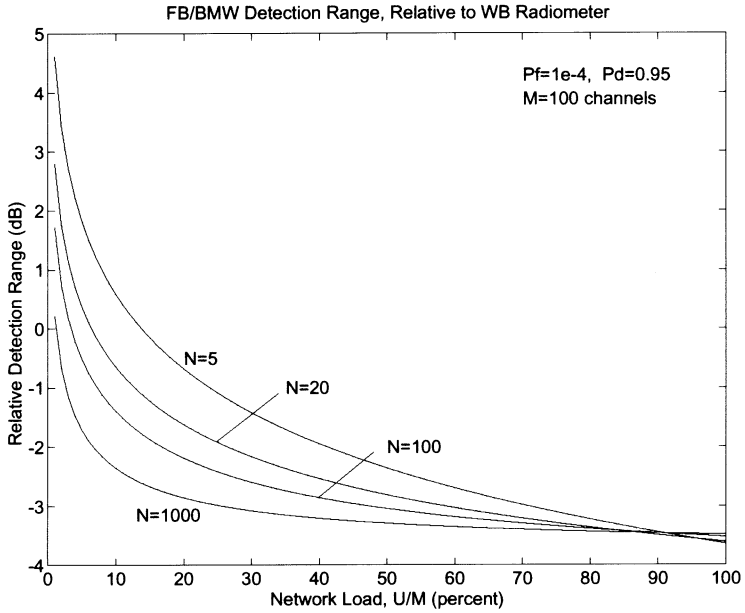

Fig. 7. Effect of network load on detection ranges, $M = 100$.

threat to the LPI network. The channelized detector is superior only when the hop rate and network load are small. LPI network waveforms should therefore be designed such that detection with the radiometer is minimized. M and N can then be selected, based on the expected number of users U such that the channelized detector performs no better than the radiometer.

B. Reducing Network Detectability

In this section we consider how the network waveforms can be designed such that the overall network detectability is reduced. First, it is important to distinguish between the design of LPI links and networks. In the design of an LPI link, the waveforms (and all other system parameters for that matter) can be adjusted to obtain minimum detectability. However, there is less freedom in designing waveforms for an LPI network, since the network waveform is usually dictated by the multiple access structure. Hence, any waveform design changes to enhance LPI must be compatible with the given multiple access scheme, which limits the freedom available to any given network emitter to adjust its signal parameters. For example, in the FH-CDMA network, a network user cannot arbitrarily deviate from its assigned hop patterns, channel bandwidth,

or frequency hop rate without interfering with the other users.

Intuitively, we see that there are two ways to approach the problem: increase the required intercept SNR, or reduce the amount of energy available to the interceptor (i.e., see (21)). For some specified P_F and P_D, it is well known that the required intercept SNR can be increased by using waveforms with large time-bandwidth products. For example, consider the detection of a dispersed network with the wideband radiometer. The total received energy per noise power spectral density is illustrated in Fig. 3. An increase $(E/N_0)_{\text{req}}$ is analogous to taking higher horizontal cuts of the received SNR mesh surface, which results in a reduction in intercept area, as shown in Fig. 4. Likewise, in the stand-off intercept scenario, it is clear that the covertness of the LPI network improves as S_I/N_0 increases, as shown in (33).

Network covertness is also improved by reducing the amount of energy available to the interceptor. Assuming the broadcast ranges of the network transmitters remain unchanged, this is achieved through the use of energy-efficient waveforms and reduced data rates, which allow a reduction in transmit power while maintaining the desired bit error probability. For example, in the dispersed network scenario, reducing S_C/N_0 reduces the signal energy received from each transmitter. Hence, the surface shown in Fig. 3 is pushed down, which for a constant $(E/N_0)_{\text{req}}$ reduces the intercept area. Similarly, in the stand-off intercept scenario, a reduction in S_C/N_0 increases the network LPI quality factor, thereby improving covertness. For the remainder of this section, we focus on techniques for reducing S_C/N_0.

From (20), we see that $(E/N_0)_{\text{recv}}$ is reduced through the use of lower data rates (R_b) and efficient modulation techniques (E_b/N_0). While the waveform modulation (i.e., frequency shift keying (FSK) with frequency hopping) depends on the network multiple access structure and is somewhat fixed, error control coding and data rate control can be applied by each emitter independently. For example, nonbinary Reed–Solomon codes are well suited for use with M-ary orthogonal signaling, and are considered here. For example, with $M = 32$, a (31,23) code can be used which has a modest coding gain and reasonable overhead. This code can correct code words with up to and including four code word symbol errors.

To reduce the data rate, we use pulse combining, as discussed in [6]. Combining is preferable to simply slowing down the hop rate, since it can be employed by individual transmitters without interfering with other network users. That is, no change in the hop rate is required. If noncoherent detection and combining are used, then the required SNR for the desired P_E will be slightly higher due to noncoherent combining losses. Combining can be used in conjunction with Reed–Solomon coding, however, to counter some of the combining loss, resulting in the following expression for S_C/N_0,

$$\frac{S_C}{N_0} = \left(\frac{E_b}{N_0}\right)_1 R_b \frac{L_C}{L} \frac{1}{G_{\text{code}}(L)} \tag{40}$$

where $(E_b/N_0)_1$ is the SNR per bit required to obtain the specified P_E (without coding or combining). This SNR depends solely on the modulation and network multiple access structure (i.e., noncoherent M-ary FSK). R_b is the burst data rate, which accounts for information and coding overhead bits, L is the number of pulses/hops combined, and L_C is the corresponding combining loss. The coding gain, $G_{\text{code}}(L)$, depends on the modulation type, the Reed–Solomon code properties, noise statistics, and the channel symbol error probability, which in turn depends on L. As the combining level increases, the error correction code becomes less effective, due to the inherent inefficiency of noncoherent combining [7].

C. Example Network Detectability Analysis

We now develop two scenarios to illustrate the application of the detectability models and waveform design techniques derived earlier. The following parameters are used: $W_1 = 100$ MHz, $T_1 = 1$ s, $U = 10$, $R_C = 5$ mi, $P_E = 10^{-5}$, $R_b = 2400$ bit/s, $P_F = 10^{-4}$, and $P_D = 0.95$.

32-ary orthogonal FSK modulation with noncoherent detection is assumed. To achieve $P_E = 10^{-5}$ using 32-ary orthogonal, noncoherent FSK, $E_b/N_0 = 7.1$ dB, hence with $R_b = 2400$ bit/s, $S_C/N_0 = 40.9$ dB-Hz. A frequency hop rate of $N = 480$ hops/s is required, since each hop consists of 5 bits. $M = 100$ is used for this analysis, yielding a network load of 10%.

1) *Dispersed Network Intercept Model*: For this example, the transmitter locations $\{(x_j, y_j)\}$ are randomly distributed within a 10×10 mi region, each with range $R_C = 5$ mi. An intercept antenna gain of 0 dB is assumed. The intercept area for the radiometer and channelized radiometer are 232 and 154 square mi, respectively, showing that the radiometer poses the greater threat to this network. Detectability contours for $P_D = 0.95$ are shown in Fig. 8.

Now consider the use of noncoherent pulse combining in conjunction with Reed–Solomon coding to reduce the data rate. Using $L = 10$ with a (31,23) code results in $L_C/L = -8$ dB and a coding gain of $G_{\text{code}}(L) = 1.4$ dB. Hence, S_C/N_0 is reduced to 31.5 dB-Hz, resulting in detection areas of $R_{RAD} = 35.4$ and $R_{FB} = 29.8$ square mi, respectively. This substantial reduction in detectability for both receivers is illustrated in Fig. 8.

2) *Stand-off Network Intercept Model*: For the stand-off scenario, an intercept gain of $G_I = 10$ dB (relative to omnidirectional) is used. For 32-ary

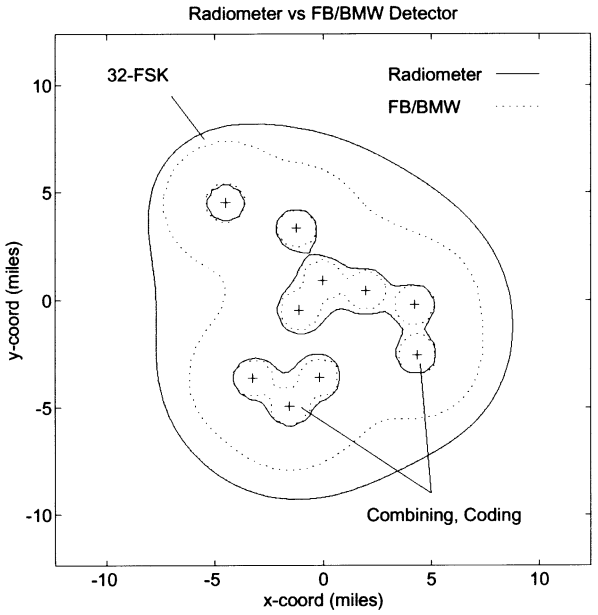

Fig. 8. Comparison of wideband and channelized radiometers.

noncoherent FSK modulation and noncoherent detection (no coding or combining), S_C/N_0 = 40.9 dB-Hz. Thus, from (33), $Q_{RAD} = -13.6$ dB, and $R_{RAD} = 24$ mi. For the channelized detector, $Q_{FB} = -9.4$ dB, and $R_{FB} = 14.8$ mi, 2.1 dB less than R_{RAD}, which agrees with Fig. 5.

With $L = 10$ combining and a (31,23) Reed–Solomon code, $S_C/N_0 = 31.5$ dB-Hz. Therefore, the radiometer's quality factor and detection range are -4.2 dB and 8.1 mi, respectively. For the channelized detector, $Q_{FB} = 0$ dB, and $R_{FB} = R_C = 5$ mi.

V. CONCLUSIONS

In this paper, two multiple access LPI network detectability models, with their corresponding performance metrics were developed. Both models provide new insight into the issues regarding detection of multiple access networks, as well as the design of waveforms for network multiple access. The dispersed network intercept model is applicable for situations in which the network transmitters are geographically dispersed throughout the tactical region of interest, and the interceptor is possibly inside the network. The model computes the probability of detection by an interceptor based on the received energy from each emitter. The performance metric for this model is the detection area for the specified probabilities of false alarm and detection. This model is highly dependent on the network scenario, such as transmitter placement.

The stand-off network intercept model was developed for situations in which the network transmitters have equal power levels and are very close together, and the interceptor is relatively far away, resulting in equal energy received from each emitter. Under these assumptions, the required SNR from each emitter can be determined as a function of the desired intercept performance, and network LPI quality factors can be used to directly compare the communication and intercept ranges of the network, as a function of the signaling waveforms. This model is scenario independent—only the waveform parameters and the methods used to detect them are important.

Several techniques for reducing the detectability of the network were also investigated, most notably data rate reduction via noncoherent pulse combining. The advantage of pulse combining is that it can be applied individually by the transmitters without disrupting other network users.

REFERENCES

[1] Dillard, R. A. (1979)
Detectability of spread-spectrum signals.
IEEE Transactions on Aerospace and Electronic Systems, **AES-15** (July 1979).

[2] Dillard, R. A., and Dillard, G. M. (1989)
Detectability of Spread-Spectrum Signals.
Norwood, MA: Artech House, 1989.

[3] Edell, J. D. (1976)
Wideband, noncoherent, frequency-hopped waveforms and their hybrids in low probability of intercept communications.
Report NRL 8025, Naval Research Laboratory, Nov. 8, 1976.

[4] Engler, H. F., and Howard, D. H. (1985)
A compendium of analytic models for coherent and noncoherent receivers.
Technical report AFWAL-TR-85-1118, Air Force Wright Aeronautical Laboratory, Sept. 1985.

[5] Gutman, L. L., and Prescott, G. E. (1989)
System quality factors for LPI communication.
IEEE Aerospace and Electronic System Magazine (Dec. 1989), 25–28.

[6] Mills, R. F., and Prescott, G. E. (1993)
Noncoherent pulse combining for improved multiple access LPI network performance.
In *Proceedings of the 1993 IEEE Military Communications Conference* (MILCOM-93), Oct. 1993.

[7] Proakis, J. G. (1989)
Digital Communications.
New York: McGraw-Hill, 1989.

Robert F. Mills was born in Spokane, WA, in 1960. He received a B.S. degree in electrical engineering at Montana State University, Bozeman, in 1983, graduating with highest honors. In 1987, he was a distinguished graduate at the Air Force Institute of Technology, Wright-Patterson Air Force Base, OH, where he received his M.S. degree, also in electrical engineering. In 1994, he was awarded a Ph.D. in electrical engineering from the University of Kansas, Lawrence.

In June 1982, he enlisted in the United States Air Force, and upon completion of his undergraduate degree, he received a commission as a Second Lieutenant from Officer Training School, Lackland AFB, TX. He currently holds the rank of Lieutenant Colonel, and is assigned to the Joint Analysis Center at Royal Air Force (RAF) Molesworth, United Kingdom, where he directs over 200 people in the day-to-day operations and maintenance of numerous intelligence support systems and an information technology architecture used throughout the European theatre of operations. His previous assignments include assistant professorship at the Air Force Institute of Technology, radar evaluation at Hill AFB, UT, and communications system engineering at Tinker AFB, OK. His research interests include digital communications, low-probability-of-intercept/anti-jam communications techniques, and signal processing.

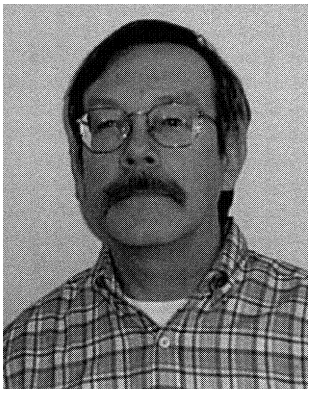

Glenn E. Prescott (S'84—M'84—SM'89) is currently Professor of Electrical and Computer Engineering at the University of Kansas where he teaches and conducts research in the areas of digital signal processing, information theory, and digital communications. He is an active researcher with the University of Kansas Telecommunications and Information Sciences Lab and the Radar and Remote Sensing Laboratory. His primary areas of research are military communication systems, low probability of intercept/interference waveform design, spread spectrum modulation techniques, and radio modem design.

Dr. Prescott has served as a publication reviewer for the IEEE Communications Society and the National Science Foundation. He is also Vice President of Lawrence Applied Research Corporation, which is involved in defense related consulting activities.